CHEMIJA
2026. Vol. 37. No. 2. P. 108–125

ISSN 0235-7216 eISSN 2424-4538
DOI: https://doi.org/10.6001/chemija.2026.37.2.3

MOF-derived materials for photoelectrochemical water splitting: design principles, mechanisms, and solar-to-hydrogen applications

Min Mei[1*],

Wenjing Yang[2]

[1] *Hunan College for Preschool Education, Changde, Hunan, 415000, P. R. China*

[2] *College of Materials Science and Engineering, Taiyuan University of Technology, Taiyuan, Shanxi, 030024, P. R. China*

The development of sustainable hydrogen production technologies is central to addressing the global energy crisis and mitigating climate change. Among available strategies, photoelectrochemical (PEC) water splitting stands out as a promising route for direct solar-to-fuel conversion, though it remains hindered by poor light absorption, charge recombination, and sluggish surface reaction kinetics. Metal-organic framework (MOF)-derived materials have emerged as versatile candidates to overcome these bottlenecks, offering tunable compositions, high surface areas, and well-defined morphologies. This review critically examines the design and synthesis strategies employed to transform MOF precursors into functional photoelectrodes, including controlled pyrolysis, calcination, heterostructure engineering, and defect modulation. Special emphasis is placed on the mechanistic insights into charge carrier generation, separation and transport, highlighting the debate surrounding the identity of the true active sites, whether nanoparticles, N-doped carbon, or single-atom centres. Performance benchmarking demonstrates that MOF-derived photoanodes and photocathodes can achieve photocurrent densities exceeding 5 mA cm^{-2} in three-electrode PEC configurations, while device-level STH efficiencies (>10%) are achieved only when these materials function within unbiased two-electrode architectures (PEC tandems or PV–electrolysis tandems) where the full photovoltage is supplied by paired absorbers and/or integrated photovoltaics. To avoid ambiguity, this review now reports STH only for unbiased device demonstrations, and reports ABPE (applied-bias photon-to-current efficiency) or other electrode-level metrics for half-cell photoelectrode studies. The review also underscores the challenges of stability, scalability, and standardised testing protocols, while showcasing promising trends such as operando characterisation, defect engineering, and artificial intelligence (AI)-assisted material discovery. By mapping current advances and future perspectives, this work provides a comprehensive overview of how MOF-derived systems can accelerate the transition to efficient and durable PEC water splitting technologies.

Keywords: heterostructures, charge carrier dynamics, surface catalysis, defect engineering, solar fuel devices

INTRODUCTION

The escalating global energy demand and the pressing realities of climate change, driven primarily by the combustion of fossil fuels, have catalysed an urgent, worldwide search for clean and sustainable energy alternatives [1]. Among the most promising solutions is the development of a green hydrogen economy, where hydrogen gas (H_2) serves as a high-energy-density, carbon-free fuel [2]. Photoelectrochemical (PEC) water splitting represents a particularly elegant and direct pathway to this goal,

* Corresponding author. Email: maynmin@163.com

utilising semiconductor materials to capture solar energy and drive the decomposition of water into hydrogen and oxygen (O_2). This process offers a direct conversion of solar to chemical energy, storing the intermittent energy of sunlight in the chemical bonds of hydrogen fuel.

Despite its conceptual promise, the practical realisation of large-scale PEC water splitting is impeded by several fundamental materials science challenges. The efficiency of the process is fundamentally limited by three critical bottlenecks. First, many robust and stable semiconductor materials, such as titanium dioxide (TiO_2), possess wide bandgaps that only allow them to absorb the ultraviolet portion of the solar spectrum, wasting the majority of available solar energy. Second, even when photons are successfully absorbed to create electron-hole pairs, these charge carriers are prone to rapid recombination, often on the timescale of picoseconds to nanoseconds, releasing their energy as heat or light before they can participate in chemical reactions at the electrode surface [3]. Third, the surface redox reactions themselves – the four-electron oxygen evolution reaction (OER) at the photoanode and the two-electron hydrogen evolution reaction (HER) at the photocathode – are kinetically sluggish and require significant overpotentials to proceed at meaningful rates, further reducing overall efficiency [4].

In the quest for materials that can overcome these hurdles, metal-organic frameworks (MOFs) have emerged as a uniquely versatile platform. MOFs are crystalline, porous materials constructed from metal ions or clusters (nodes) linked by organic molecules (linkers) [3]. Their defining characteristic is their near-infinite tunability; by judiciously selecting from a vast library of available metal nodes and organic linkers, it is possible to rationally design materials with a precise control over pore size, topology, specific surface area, and chemical functionality [5]. This modularity offers an unprecedented potential for creating highly ordered structures tailored for catalytic applications. However, the very properties that make pristine MOFs structurally elegant often render them unsuitable for direct use as photoelectrodes. The majority of MOFs suffer from a poor intrinsic electrical conductivity, which hinders the efficient transport of charge carriers to the surface, and a pronounced lack of stability in aqueous electrolytes, particularly under the harsh, prolonged illumination and electrochemical bias required for water splitting [6]. This has led to a paradigm shift in the field: instead of using MOFs directly, researchers are increasingly employing them as sacrificial templates or precursors to create a new class of MOF-derived materials [4]. Through controlled thermal or chemical transformation, the ordered structure of the parent MOF is converted into highly functional nanomaterials, including porous metal oxides, sulfides, phosphides, carbides, and metal nanoparticles embedded within a porous carbon matrix. This strategic derivatisation process aims to combine the best attributes of two distinct material classes. The derived materials often inherit the high surface area, well-defined porosity, and complex morphology of the MOF template, while simultaneously gaining the enhanced electronic conductivity and the superior chemical and thermal stability characteristic of inorganic materials [7]. This approach navigates a fundamental trade-off: the thermal decomposition required to impart stability and conductivity inherently disrupts the perfect, long-range crystalline order of the parent MOF. The central challenge, and the focus of much current research, is to manage this transformation to maximise the retention of beneficial templated nanostructures while achieving the necessary electronic and stability enhancements for high-performance photoelectrocatalysis.

This review provides a critical and comprehensive analysis of the rapidly advancing field of MOF-derived materials for PEC water splitting. We begin by examining the key design principles and synthesis strategies that enable the conversion of MOF precursors into functional photoelectrodes with controlled composition and morphology. We then delve into the mechanistic underpinnings of their photoelectrocatalytic activity, exploring charge carrier dynamics and critically analysing the ongoing debate surrounding the nature of the true active sites. Subsequently, we benchmark the performance of state-of-the-art MOF-derived photoanodes and photocathodes, discussing their integration into complete solar-to-hydrogen (STH) conversion devices. Finally, we offer a forward-looking perspective on the overarching challenges – particularly the activity-stability trade-off – and highlight emerging trends that will shape the future of this promising field.

DESIGN AND SYNTHESIS STRATEGIES FOR MOF-DERIVED PHOTOELECTRODES

The transition from a well-defined MOF precursor to a high-performance photoelectrode is not a trivial decomposition but a sophisticated materials engineering process. The success of this transformation hinges on the precise control of synthetic parameters to dictate the final composition, nanostructure, and interfacial properties of the derived material. This section critically evaluates the key strategies employed in the design and synthesis of MOF-derived photoelectrodes, from thermal conversion protocols to the engineering of complex hierarchical architectures.

Controlled thermal transformation: from precursor to functional material

Thermal treatment, primarily in the form of pyrolysis (in an inert atmosphere) or calcination (in an oxidising atmosphere), stands as the most prevalent and powerful method for converting MOF precursors into functional inorganic materials [8]. The choice of thermal conditions is a critical design parameter that directly determines the chemical nature of the final product. Pyrolysis under an inert atmosphere, such as nitrogen or argon, causes the organic linkers to decompose into a porous carbon matrix, while the metal nodes are reduced to form metallic, carbide, phosphide, or sulfide nanoparticles embedded within this matrix [9]. As illustrated in Fig. 1, which schematically contrasts the thermal transformation pathways, this anaerobic treatment preserves the carbon content to generate conductive composites, whereas aerobic calcination removes the organic framework to yield porous metal oxides. This approach is particularly effective for creating HER catalysts, where the conductive carbon matrix facilitates electron transport and the embedded nanoparticles act as catalytic sites. For example, pyrolysis of an iron-containing MOF yielded unique iron oxide@iron carbide core-shell nanoparticles dispersed on a carbon support, a structure highly favourable for catalysis [10]. In stark contrast, calcination in an oxidising atmosphere like air results in the complete combustion of the organic linkers, leaving behind a porous network of metal oxide

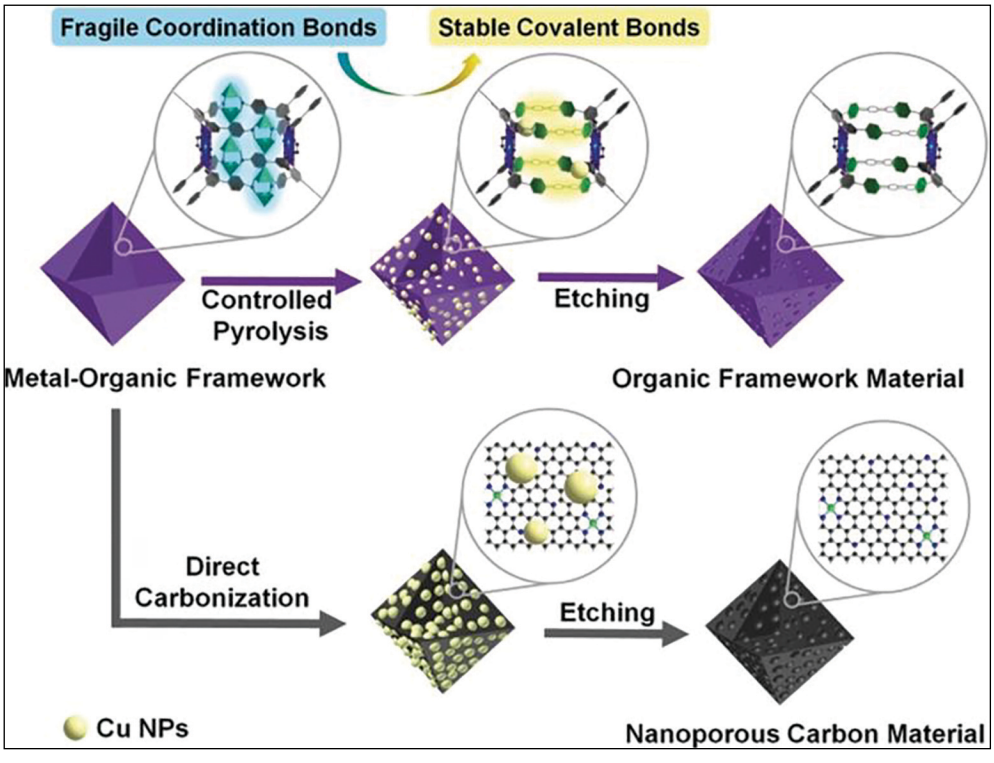

Fig. 1. Schematic illustration of the transformation of a generic MOF precursor into different derived materials [14]. Pyrolysis in an inert atmosphere yields metal or metal-compound nanoparticles embedded in a porous carbon matrix, while calcination in an oxidising atmosphere produces porous metal oxides. The final product's composition and morphology are dictated by the precursor MOF and the thermal treatment conditions

nanoparticles that often retains the morphology of the parent MOF crystal [11]. This method is the primary route to fabricating photoanodes such as TiO_2, Fe_2O_3 and ZnO. The pyrolysis temperature is another crucial variable, directly influencing the degree of carbon graphitisation, the crystallinity of the inorganic phase, and the size of the resulting nanoparticles. Insufficient temperature may lead to incomplete conversion, while excessively high temperatures can cause undesirable sintering of nanoparticles and collapse of the porous structure, reducing the active surface area [8].

The rational design of a MOF-derived catalyst begins long before the furnace is turned on; it starts with the selection of the parent MOF itself. The choice of metal node is the primary determinant of the final inorganic component and its semiconducting properties. For instance, Ti-based MOFs like MIL-125 are logical precursors for TiO_2 photoanodes, while Fe-based MOFs such as MIL-88 are used to generate Fe_2O_3 [1]. The organic linker also plays a vital role. Linkers containing nitrogen atoms, such as the 2-methylimidazole in zeolitic imidazolate frameworks (ZIFs), are particularly valuable because upon pyrolysis they yield a nitrogen-doped carbon matrix. These N-dopants are not passive; they can enhance conductivity and create catalytically active sites for electrochemical reactions [12]. An advanced strategy involves the use of bimetallic or multimetallic MOFs as precursors. By incorporating two or more different metals into the MOF structure at an atomic level, subsequent pyrolysis can yield finely dispersed alloys or mixed-metal oxides. These bimetallic materials often exhibit synergistic effects, where the interplay between the two metals leads to electronic properties and catalytic activities superior to those of their single-metal counterparts [13].

Nanostructure and morphology engineering

One of the most compelling advantages of using MOFs as sacrificial templates is the remarkable ability to preserve the precursor's morphology in the final derived material. This templating effect provides a powerful tool for fabricating complex and hierarchical nanostructures that are otherwise challenging to synthesise. By controlling the morphology of the initial MOF crystal, researchers can engineer the architecture of the final photoelectrode to optimise light absorption, charge transport, and surface reaction kinetics. This strategy has been used to create a diverse library of nanostructures, spanning from zero-dimensional (0D) quantum dots to complex three-dimensional (3D) assemblies.

Prominent examples include the synthesis of hollow nanocages, often derived from polyhedral ZIF precursors like ZIF-8 and ZIF-67 (Fig. 2) [15]. These hollow structures are highly advantageous for PEC applications as they enhance light harvesting through multiple scattering events within the cavity and provide a large, accessible surface area for both electrolyte penetration and catalyst loading [16]. When a ZIF-67 precursor is converted into a hollow dodecahedral NiCo-layered double hydroxide (LDH) OER layer on $BiVO_4$, the photoanode delivers 4.54 mA cm^{-2} at 1.23 V reversible hydrogen electrode (RHE) (≈3.3 × vs bare $BiVO_4$) with an incident photon-to-current efficiency (IPCE) of 44.25% at 400 nm and applied bias photon-to-current efficiency (ABPE) of 1.12%, underscoring how intracavity multiple scattering and accessible shells translate into real gains in carrier injection and surface kinetics [17]. Complementarily, hollow-derived sulfides from ZIF-67 (CoS) used as a cocatalyst on $BiVO_4$ push the photocurrent to 5.22 mA cm^{-2} at 1.23 V_RHE by raising active-site density and conductivity-numbers that benchmark how 'voided' architectures plus electronically conductive shells can jointly advance PEC OER [18].

One-dimensional (1D) nanostructures, such as nanowires and nanorods, have also been successfully fabricated by templating from needle-shaped MOF crystals [12]. The key benefit of 1D morphologies is their ability to provide direct, continuous pathways for electron transport along the long axis, which minimises charge recombination at grain boundaries and improves charge collection efficiency [19]. ZnO@ZIF-8/67 nanorod arrays achieve 0.11 mA cm^{-2} at 1.23 V_{RHE}, about 9.2 × higher than their undressed ZnO counterpart under visible-light operation – an absolute current still modest but a clear demonstration that axial, grain-boundary-sparse pathways cut recombination and lift IPCE in the visible tail [20]. Likewise, converting ZIF-67 deposited on TiO_2 into Co_3O_4–TiO_2 heterojunctions yields 2.4 mA cm^{-2} (≈2.6 × over pristine TiO_2), directly tying 1D carrier highways and MOF-derived interfacial fields to higher charge-collection efficiency [21].

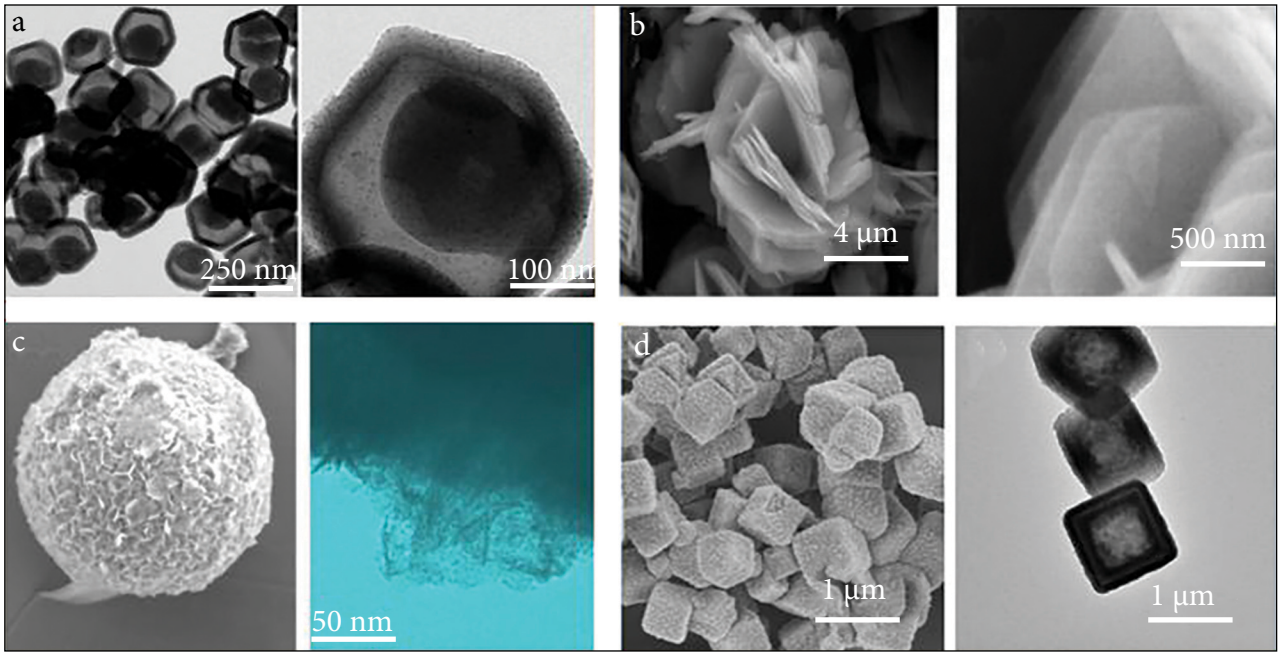

Fig. 2. A collage of scanning electron microscopy (SEM) and transmission electron microscopy (TEM) images showcasing the morphological diversity of MOF-derived materials. (a) Hollow carbon nanocages derived from ZIF-8 precursors [22]. (b) 3D flower-like hierarchical structures of NiO assembled from nanosheets [23]. (c) 2D nanosheets of Ni-Co layered double hydroxide derived from a 2D MOF [24]. (d) $CoSe_2$/carbon nanotube composites derived from Co-MOF-74 [25]

At the other end of the dimensional spectrum, 2D nanosheets, derived from layered MOF precursors, offer an extremely high surface-to-volume ratio. This morphology maximises the exposure of catalytically active sites to the electrolyte and drastically shortens the diffusion path for photogenerated charge carriers to reach the surface, thereby suppressing bulk recombination [26]. Depositing 2D Co-MOF nanosheets on $BiVO_4$ raises the photocurrent to ~6.0 mA cm^{-2} at 1.23 V_{RHE} (≈4 × vs bare), consistent with suppressed surface recombination and better band-edge energetics for hole transfer [27]. More complex, 3D hierarchical architectures, such as flower-like microspheres assembled from nanosheets, combine the benefits of both 2D and 3D structures, offering a high surface area along with a robust, interconnected porous network that facilitates mass transport [28]. The ability to rationally design and synthesise these diverse morphologies through MOF-templating represents a significant advance in the creation of next-generation photoelectrode materials.

Heterostructure construction for enhanced charge separation

While morphology engineering can optimise light absorption and charge transport, achieving a highly efficient charge separation often requires the deliberate construction of heterostructures, in which a MOF-derived phase forms an electronically coupled interface with a second component (semiconductor, cocatalyst, or conductor). In such architectures, charge separation is governed by band alignment and Fermi-level equilibration: upon contact, interfacial band bending and/or an internal electric field develops, which biases photogenerated electrons and holes toward different spatial regions and thereby suppresses bulk/surface recombination. In a Type-II heterojunction (Fig. 3a), staggered band edges drive electrons to accumulate in the lower-lying conduction band and holes in the higher-lying valence band of the partner semiconductor, producing spatial separation but potentially sacrificing redox driving force if the band offsets are large. In contrast, a Z-scheme heterojunction (Fig. 3b) intentionally recombines the 'weak' carriers (electrons in the less-negative CB and holes in the less-positive VB), retaining the strongly reducing electrons and strongly oxidising holes, which is why Z-scheme designs often improve PEC kinetics without compromising reaction thermodynamics; MOF-derived Z-scheme systems have been explicitly demonstrated for enhanced PEC water splitting when MOF-to-oxide conversion is coupled with defect/

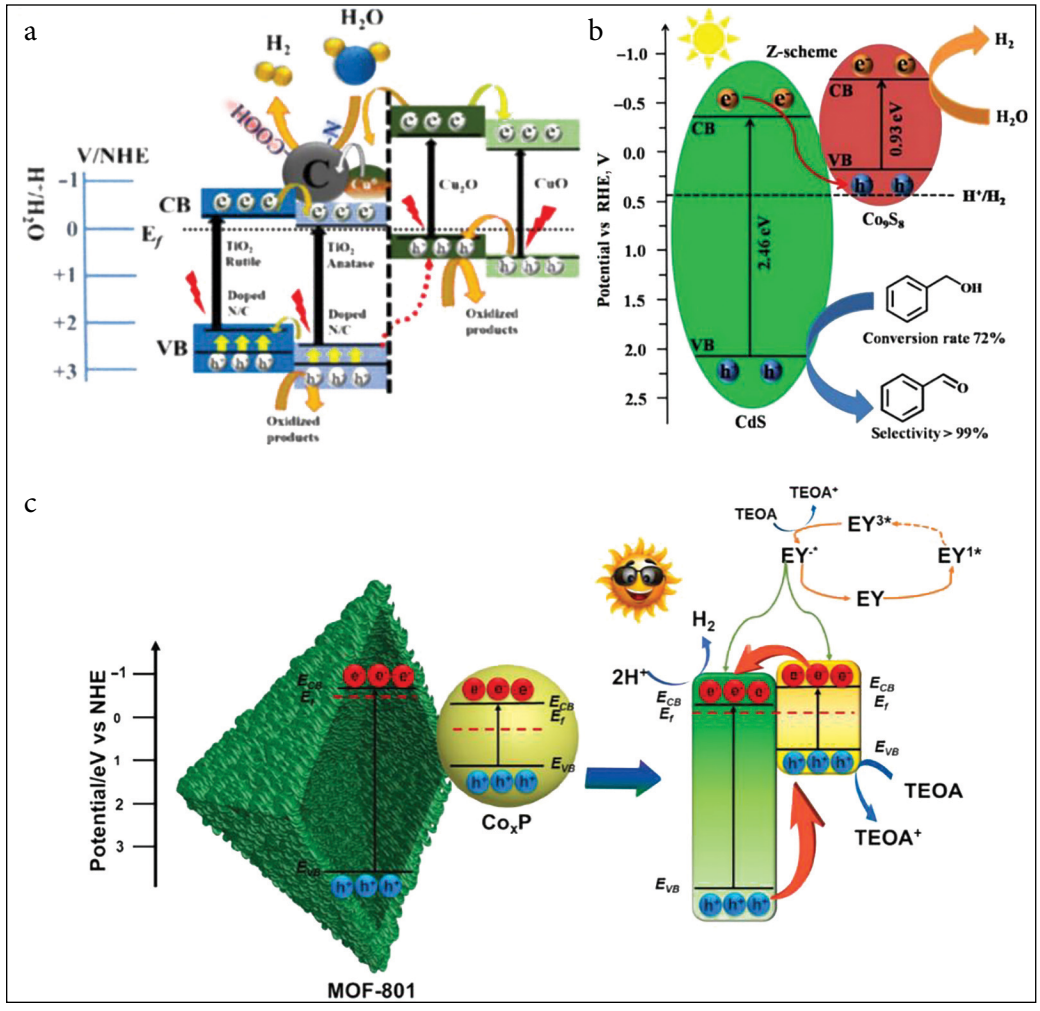

Fig. 3. Charge-separation pathways enabled by heterojunction engineering in MOF-derived PEC systems (schematic reproduced from the cited literature). (a) Type-II (staggered) heterojunction: electrons relax to the lower-lying CB of one component while holes accumulate in the higher-lying VB of the other, yielding spatial separation but potentially lowering the effective redox driving force depending on band offsets [13]. (b) Z-scheme heterojunction: the interfacial recombination channel consumes the low-energy carriers (e^- in the less-negative CB and h^+ in the less-positive VB), preserving strongly reducing electrons and strongly oxidising holes for HER/OER, thereby maintaining high redox potentials while improving separation [36]. (c) p–n heterojunction: Fermi-level equilibration forms a depletion region and built-in electric field that drives directional carrier drift across the junction and suppresses recombination [37]

vacancy engineering to accelerate interfacial transfer [29]. In a p–n heterojunction (Fig. 3c), the junction is formed by contacting p-type and n-type materials, and the resulting depletion region establishes a strong built-in electric field that promotes directional carrier drift; MOF-derived p–n interfaces (e.g. Co_3O_4 coupled with n-type oxides) are widely used to enhance hole extraction at photoanodes and reduce interfacial charge-transfer resistance [30].

From a synthesis standpoint, the interfacial quality required for these mechanisms is most reliably achieved by *in situ* MOF growth/deposition on the photoabsorber followed by controlled conversion, because it minimises interfacial voids and trap-rich boundaries. Practically, this is implemented through (i) surface growth/adsorption of a MOF layer on oxide nanorods or films (often aided by electrostatic interactions or seeded growth), followed by (ii) calcination (to form porous oxides) or anion-exchange/thermal sulfidation/selenisation/phosphidation (to form conductive chalcogenides/phosphides) while preserving conformal contact. For example, ZIF-67 can be adsorbed onto TiO_2 nanorods and annealed in air to produce a Co_3O_4/TiO_2 heterostructure photoelectrode, illustrating a representative MOF-derived p–n junction

fabrication route that couples an intimate contact with controlled phase evolution [30]. Likewise, growing ZIF-67 on a $BiVO_4$ photoanode and then calcining or sulfurising it transforms ZIF-67 into Co_3O_4 or CoS, respectively [18], enabling either junction-driven separation (band bending) and/or cocatalyst-driven kinetic acceleration depending on the final phase and thickness.

Finally, when the second component is a 2D conductor (graphene/rGO/MXene), the dominant mechanism is often rapid interfacial extraction rather than semiconductor–semiconductor band staggering: the conductor provides a low-resistance percolation network (an 'electron/hole highway') that shortens the carrier residence time in the absorber and lowers recombination probability. In Co-MOF/MXene/$BiVO_4$ photoanodes, for instance, the reported charge-separation and surface-reaction efficiencies improved substantially (≈78 and ≈89%, respectively), consistent with built-in-field-assisted directional transport across the MOF/MXene/semiconductor interfaces and reduced interfacial impedance [31]. This synthesis–mechanism linkage clarifies why the same MOF precursor strategy can yield different junction physics (Type-II vs Z-scheme vs p–n vs conductor-assisted extraction) depending on conversion chemistry, interfacial microstructure, and the electronic nature of the coupled component.

Another powerful approach involves creating composites of MOF-derived materials with highly conductive scaffolds, particularly 2D materials like graphene, reduced graphene oxide (rGO), or MXenes [32]. These 2D materials act as 'electron highways' or acceptors. When a MOF-derived semiconductor is excited by light, electrons in its conduction band can be rapidly transferred to the adjacent conductive 2D sheet. This swift extraction of electrons effectively separates them from the holes left behind in the semiconductor, prolonging their lifetime and increasing the probability of their participation in the HER at the cathode [32]. Quantitatively, the benefit of incorporating such conductive scaffolds is striking. For instance, when only 1 wt% rGO was integrated into a Zn-doped CeO_2 photoanode derived from a Ce-based MOF, the photocurrent density at 1.23 V_RHE increased to 2.23 mA cm^{-2}, nearly double that of Zn–CeO_2 without rGO and over six times higher than pristine CeO_2. This demonstrates that even minimal incorporation of rGO can dramatically improve interfacial charge separation and transport, while excessive loading leads to an undesirable optical shielding and an increased series resistance [33].

The synthesis of these heterostructures is a multi-variable optimisation problem. The final performance depends not only on the choice of the MOF precursor and the semiconductor substrate but also on the precise control over the transformation conditions that dictate the final composition, crystallinity, and, most importantly, the quality of the interface between the components. A poorly formed interface with numerous defects can act as a recombination centre, negating the benefits of the heterojunction. Therefore, a holistic design approach that considers the entire synthesis process, from precursor selection to final device fabrication, is essential for creating high-performance composite photoelectrodes. For example, ZIF-67 transformed into Co_3O_4 and coupled with TiO_2 produced a photocurrent density of 2.4 mA cm^{-2} at 1.85 V_RHE, with the onset potential reduced from 0.59 to 0.46 V_{RHE}. Although this marked improvement originated from the p–n heterojunction formation, it remained limited by bulk charge transport and recombination at defective interfaces, illustrating that MOF-derivation alone cannot match the interfacial conductivity gains offered by 2D scaffolds [34]. A holistic design approach must therefore prioritise interface engineering. A case in point is the Co-MOF/MXene/$BiVO_4$ composite, where the incorporation of Ti_3C_2 MXene as a hole-extraction layer enhanced both charge-separation and surface-reaction efficiencies to approximately 78 and 89%, respectively. The synergy resulted from the matched work functions and built-in fields at the MOF/MXene/semiconductor interfaces, which reduced interfacial impedance and promoted directional charge migration [35]. Such results underscore that MXenes not only act as conductive bridges but also actively tune band alignment and surface energetics.

While rGO enables fast electron extraction with low loadings, over-integration introduces parasitic absorption, diminishing light harvesting. Similarly, MOF-derived heterostructures without conductive 2D layers, though capable of forming favourable junctions, often suffer from transport bottlenecks and trap-induced recombination. MXenes, on the other hand, offer a dual advantage: conductivity comparable to metals and tunable surface chemistry for band alignment, yet their susceptibility to oxi-

dation may compromise long-term stability. These contrasting outcomes highlight that effective composite design is not a matter of simply adding more 2D material but of tailoring the precursor chemistry, transformation pathway, and interfacial architecture to balance optical absorption, charge separation, and durability. Future advances will hinge on coupling precise synthetic control with *in situ* characterisation to reveal how interfacial defect density, surface terminations, and conductivity percolation thresholds govern solar-to-hydrogen conversion efficiency. To consolidate the strategies discussed, Table 1 provides an illustrative summary of representative MOF-derived photoelectrode materials from the recent literature. The table highlights the critical link between the initial design choices – including the selection of the parent MOF and its metallic and organic components – and the final outcome. It details the specific derivatisation methods, key synthesis parameters like temperature and atmosphere, and the resulting composition and unique structural features of the final materials, such as hollow dodecahedra or core-shell nanowires. This compilation underscores the versatility of the MOF-templating approach for engineering a diverse range of functional nanomaterials tailored for high-performance photoelectrochemical applications.

MECHANISTIC INSIGHTS INTO PHOTOELECTROCATALYTIC PROCESSES

Understanding the fundamental mechanisms that govern the performance of MOF-derived photoelectrodes is paramount for their rational design and optimisation. The journey from photon absorption to hydrogen production involves a complex sequence of photophysical and electrochemical events, including charge carrier generation, separation, transport, and surface catalysis. This section delves into these processes, leveraging advanced characterisation techniques to elucidate the dynamics of charge carriers and critically examining the ongoing scientific debate surrounding the identity of the true catalytically active sites.

Probing charge carrier dynamics

The efficiency of any PEC device is fundamentally dictated by the fate of the photogenerated electron–hole pairs. This fundamental process is schematically outlined in Fig. 4, which traces the charge

Table 1. **Synthesis strategies for MOF-derived photoelectrode materials**

Precursor MOF	Derivatisation method	Key parameters	Resulting material	Key structural features	Reference(s)
ZIF-67 (Zeolitic Imidazolate Framework-67; cobalt(II) coordinated with 2-methylimidazolate ligands; commonly written as $Co(2\text{-mIm})_2$)	Pyrolysis	700°C, Ar	Co@N-doped carbon	Hollow dodecahedra	[38]
NH_2-MIL-125(Ti/Cu) (Amino-functionalised MIL-125(Ti) constructed from $Ti_8(OH)_4$ clusters and 2-aminoterephthalate linkers; Cu incorporated as secondary metal species)	Pyrolysis	Ar/H_2O vapour	TiO_2/CuxO/C	Anatase/rutile nanocomposite	[13]
Ni-BTC MOF (Nickel 1,3,5-benzenetricarboxylate framework; synthesised from $NiCl_2{\cdot}6H_2O$ and H_3BTC (1,3,5-benzenetricarboxylic acid))	Pyrolysis	800°C, N_2	Ni/NiO@porous carbon	Hierarchical hollow spheres	[39]
ZIF-67-derived NiCo LDH precursor ($Co(2\text{-methylimidazolate})_2$ transformed via $Ni(NO_3)_2$ hydrothermal treatment into NiCo layered double hydroxide)	Selenylation	400°C, Ar	$NiSe_2$–$CoSe_2$@C	Core-shell on MXene	[40]
MIL-101(Fe) (Materials of Institut Lavoisier-101(Fe); commonly formulated as $Fe_3O(OH)(H_2O)_2(BDC)_3$, where BDC = benzene-1,4-dicarboxylate)	Calcination	500°C, Ar	Porous Fe_2O_3	Spindle-like morphology	[41]
ZIF-8 (Zeolitic Imidazolate Framework-8; zinc(II) coordinated with 2-methylimidazolate ligands; commonly written as $Zn(2\text{-mIm})_2$)	Pyrolysis + leaching	900°C, N_2	N-doped porous carbon	High surface area carbon	[42]
MOF-74(Ni) (Nickel-MOF-74; typically described as Ni_2(dobdc), where dobdc = 2,5-dihydroxyterephthalate)	Microwave + laser	Laser irradiation	NiO nanoparticles in carbon	Hierarchical structure	[43]
Hofmann-type (Co, W)-MOF (Hofmann-type coordination framework containing Co and W metal centre bridged by cyanide ligands)	Pyrolysis + sulfidation	450°C, H_2S/Ar	S-CoWP@(S,N)-C	Nanowires	[12]

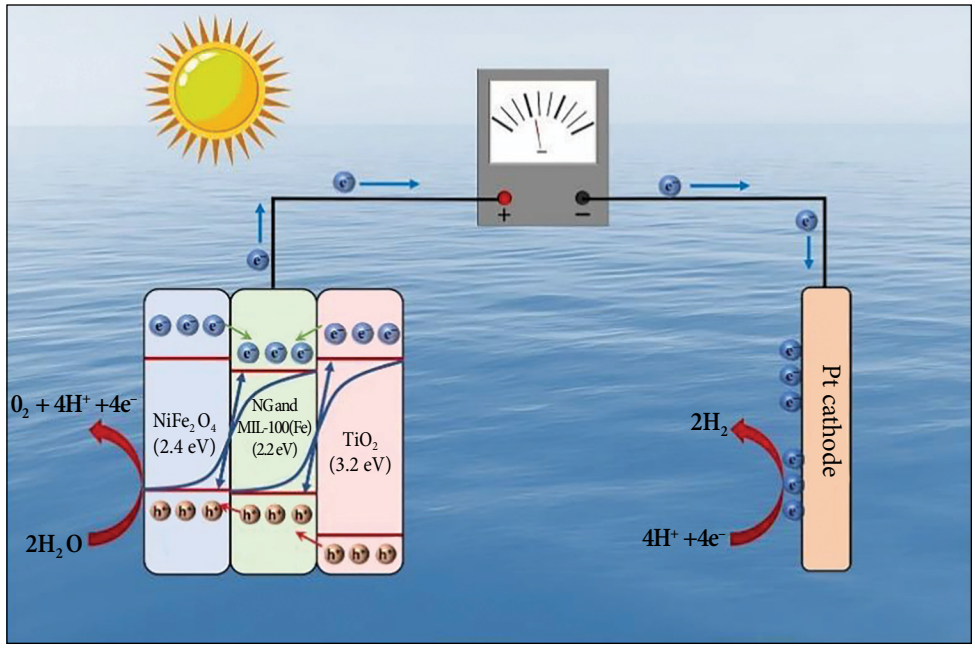

Fig. 4. Schematic diagram of the fundamental processes in a MOF-derived heterojunction photoanode for PEC water splitting [46]

carrier journey from initial photon absorption and exciton generation to the final surface redox reactions. Upon absorbing a photon with energy greater than its bandgap, the MOF-derived semiconductor generates an exciton, which must then separate into a free electron and hole that migrate to opposite ends of the device [44]. The principal challenge is that the timescale for recombination is often much faster than that for charge transport and surface reactions. MOF-derived materials, especially those engineered into heterostructures, are designed to manipulate these timescales favourably. The built-in electric fields at interfaces, such as those in p-n or Type-II heterojunctions, provide a strong driving force for the rapid spatial separation of electrons and holes, moving them apart before they can recombine [13].

Direct evidence for these dynamic processes comes from advanced time-resolved spectroscopic techniques. Transient absorption spectroscopy (TAS) is a powerful tool that acts like a high-speed camera, allowing researchers to monitor the population of excited states and separated charge carriers on timescales from femtoseconds to milliseconds [26]. Studies using TAS have provided crucial insights; for example, the analysis of a Ru-catalyst-embedded MOF on a WO_3 semiconductor revealed a key hole transfer process from the excited WO_3 to the MOF, a critical step in the charge separation pathway [45]. Such measurements can quantify the lifetime of separated charges, demonstrating that well-designed heterostructures can extend this lifetime by orders of magnitude, providing a much larger window for the charges to reach the electrode surface and drive water splitting reactions.

Complementing TAS, electrochemical impedance spectroscopy (EIS) provides vital information about the kinetics of charge transfer at the solid–liquid interface [26]. In a typical EIS experiment, the impedance of the photoelectrode is measured as a function of frequency, often represented in a Nyquist plot. Figure 5 presents representative Nyquist plots contrasting a bare semiconductor with a MOF-modified photoanode; the significant reduction in the semicircle diameter for the modified electrode visually confirms a decrease in the charge transfer resistance (Rct). The diameter of the semicircle in this plot corresponds to the charge transfer resistance (Rct), which represents the kinetic barrier for transferring an electron or hole from the electrode surface to an acceptor/donor molecule (e.g. water) in the electrolyte [47]. A significant and recurring finding in the literature is that modifying a semiconductor with a MOF-derived cocatalyst leads to a dramatic reduction in Rct. This indicates that the MOF-derived layer provides more efficient

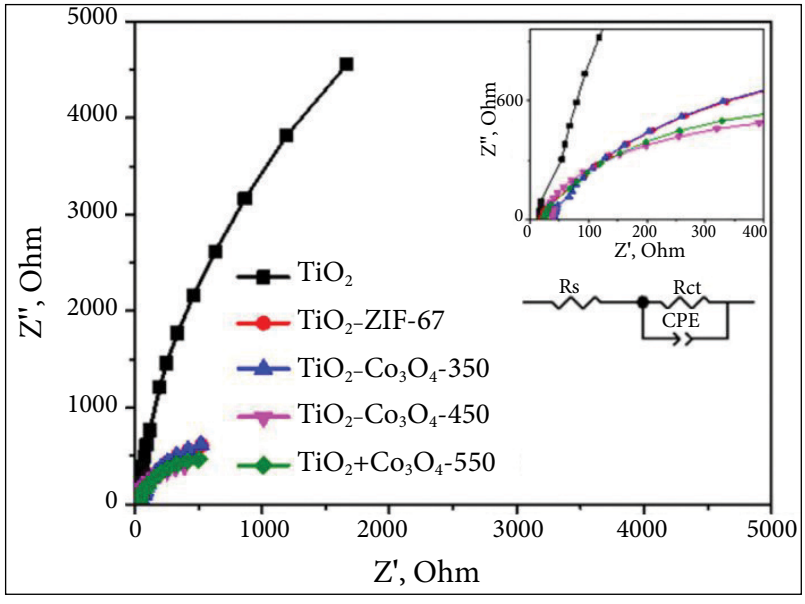

Fig. 5. Representative Nyquist plots from EIS comparing a bare semiconductor photoanode with the same photoanode modified with a MOF-derived cocatalyst layer. The significantly smaller semicircle for the modified electrode indicates a lower Rct [34]

catalytic sites that accelerate the surface redox reaction, allowing charge transfer to effectively outcompete surface recombination processes.

Beyond the qualitative trends from TAS and EIS, the literature provides several quantitative examples that illustrate how MOF-derived layers tune *specific* kinetic bottlenecks (interfacial transfer, recombination suppression, defect passivation, and surface catalysis). To improve clarity, we separate five representative case studies below and briefly state the dominant mechanistic lever highlighted by each dataset.

Case 1 (spectroscopy-defined interfacial hole transfer): In a MOF/semiconductor composite where a Ru-functionalised UiO-type MOF is integrated with WO_3, transient absorption analysis (485 nm) shows that the hole-relaxation components observed for bare WO_3 (4 ± 2 ps, 40 ± 20 ps, 1000 ± 200 ps and >8 ns) shift to faster components (1.5 ± 0.4 ps, 30 ± 10 ps and 600 ± 30 ps) after MOF integration, consistent with an accelerated interfacial hole extraction/transfer rather than simple lifetime extension. Importantly, the PEC selectivity/efficiency improves concurrently, with the reported initial faradaic efficiency for O_2 evolution increasing from ~66% (0.6–0.9 V vs NHE) to 84% at 1.0 V, showing that shorter spectroscopic decays can still accompany higher productive charge utilisation when interfacial transfer is improved [48].

Case 2 (triadic heterojunction + cocatalyst lowers interfacial impedance and shifts onset): For a NiFe-LDH/CdS/$BiVO_4$ photoanode, the impedance-derived charge-transfer resistance decreases substantially (from 950 Ω for $BiVO_4$ to 420 Ω for the triadic system), while the onset potential shifts cathodically by 540 mV and the photocurrent increases from 0.53 to 3.1 mA cm^{-2} under AM 1.5G illumination. These concurrent changes support a mechanism where the CdS/$BiVO_4$ junction promotes charge separation and the NiFe-LDH layer accelerates surface OER kinetics (hole transfer and catalytic turnover), thereby reducing interfacial recombination losses [49].

Case 3 (MOF thin-layer defect/oxygen-vacancy stabilisation and passivation): When a thin NiFe-MOF is conformally coated on oxygen-vacancy-rich $BiVO_4$, photocurrents of 5.3 ± 0.15 mA cm^{-2} at 1.23 V_RHE are reported alongside improved operational stability. In this architecture, the MOF layer functions not only as a cocatalyst but also as a *chemical/passivation layer* that stabilises defect chemistry and suppresses defect-mediated interfacial recombination pathways – an effect that is mechanistically distinct from simply increasing conductivity [50].

Case 4 (MOF-derived sulfide cocatalyst: conductivity + junction field suppresses recombination): Converting ZIF-67 into a MOF-derived CoS

cocatalyst on $BiVO_4$ yields a photoanode delivering 5.22 mA cm^{-2} at 1.23 V_RHE. Here, the key lever is the formation of an electronically coupled $CoS/BiVO_4$ interface where the cocatalyst provides higher conductivity and catalytic site density, while junction band-bending/built-in fields facilitate carrier separation and suppress bulk-to-surface recombination-achieving performance comparable to MOF-protective layers but via a different kinetic pathway [51].

Case 5 (interfacial electronic-structure tuning to enhance hole extraction thermodynamics): In $BiVO_4$/MnFe-MOF photoanodes, reported photocurrents reach 3.64 mA cm^{-2} at 1.23 V_RHE, attributed to interfacial bonding/electronic interactions that increase the driving force for hole extraction and improve interfacial charge separation. This example highlights that band-edge/interfacial electronic-structure engineering can rival conductivity-driven approaches by improving the thermodynamics and kinetics of hole transfer at the semiconductor/cocatalyst interface [52].

Collectively, these examples show that 'improved charge carrier dynamics' in MOF-derived PEC systems is not a single phenomenon: performance gains can arise from faster interfacial transfer, lower interfacial impedance, defect stabilisation/passivation, conductive cocatalysis with junction fields, or deliberate electronic-structure tuning. Presenting the cases separately clarifies which kinetic lever is supported by which measurement and avoids overgeneralising a single 'MOF effect' across mechanistically distinct material designs.

The controversy of the active site

Although MOF-derived photoelectrodes often show substantial gains in photocurrent and onset potential, the field continues to debate which structural motif constitutes the primary catalytic 'active site' for interfacial HER/OER. This ambiguity is expected because MOF-to-derivative transformations rarely yield a single phase; instead, they commonly generate multicomponent composites (oxide/sulfide/phosphide nanoparticles, N-doped carbon, and occasionally atomically dispersed metal species) that can each contribute to kinetics, interfacial energetics, and charge-transfer pathways under illumination. We therefore reorganise the discussion below into three dominant hypotheses and then reconcile why these motifs may coexist in a single working photoelectrode [53].

In the classical view, catalysis occurs predominantly on inorganic nanoparticles (e.g. oxides, sulfides and phosphides) that form from MOF metal nodes during calcination/pyrolysis. In this model, the nanoparticle surface provides adsorption and turnover sites for key intermediates, while the photoabsorber supplies photogenerated carriers and the MOF-derived phase primarily lowers kinetic barriers at the semiconductor/electrolyte interface. A representative example in PEC OER is the use of MOF-derived cobalt sulfide as a cocatalyst on $BiVO_4$, where the interfacial CoS layer is correlated with accelerated surface kinetics and improved charge utilisation under AM 1.5G illumination. The critical point for PEC interpretation is that, when the cocatalyst is non-photoactive, its role is primarily to increase surface reaction rates and reduce surface recombination, rather than to contribute light absorption [54].

A second viewpoint emphasises that the linker-derived carbon is not merely a conductive scaffold. When N-containing linkers are used (notably ZIF-type imidazolates), pyrolysis can produce N-doped carbon with electronically polarised carbon atoms adjacent to pyridinic/pyrrolic N. Such sites are widely discussed as catalytically relevant in electrochemical reactions because N dopants modulate local charge density and can introduce Lewis basic character at neighbouring carbon atoms; this framework provides a mechanistic basis for why carbon domains may participate directly in interfacial steps, in addition to facilitating carrier transport [55]. In MOF-derived PEC electrodes, this 'carbon effect' can manifest as reduced series resistance, altered band bending at the cocatalyst/semiconductor junction, and suppressed interfacial recombination, making it essential to distinguish purely electronic improvements from true catalytic turnover on carbon sites.

A third and rapidly developing perspective attributes activity to single-atom catalysts (SACs)-isolated metal atoms stabilised by coordination to N in a carbon matrix ($M–N_x–C$, commonly $M–N_4$). MOF chemistry is well suited to generate such motifs because metal–ligand coordination can preorganise local environments and, in bimetallic systems, volatile metals (e.g. Zn) can help create spatial separation during pyrolysis,

enabling site-isolated metal centres. A canonical demonstration of Zn-assisted synthesis of $M–N_4$ sites is the polymerisation–pyrolysis–evaporation strategy reported for Zn/Fe precursors, which illustrates how sacrificial Zn can facilitate porosity and stabilise atomically dispersed $Fe–N_4$ coordination after thermal treatment [56]. Importantly for PEC, atomically dispersed cocatalysts can reduce the optical and recombination penalties associated with thick nanoparticle overlayers while still providing a high intrinsic activity per metal atom.

A PEC-specific illustration of the SAC concept is the 'single-atomic Co' cocatalyst anchored on the (040) facet of $BiVO_4$, which was reported to deliver strongly enhanced charge-separation/charge-injection behaviour relative to nanoparticulate Co-based coatings [57]. This type of result supports the mechanistic claim that sparse, site-isolated cocatalyst centres can accelerate interfacial kinetics while minimising parasitic recombination introduced by thicker, less selective cocatalyst films.

These three assignments are not mutually exclusive because MOF-derived materials often contain hybrid motifs (nanoparticles electronically wired by N-doped carbon, plus sub-nanometer clusters and occasional single atoms). As a result, the 'dominant active site' can appear to change depending on the characterisation method (TEM vs XAS), the electrolyte, the applied bias, and illumination. Moreover, active surfaces can reconstruct during operation, so *ex situ* structures may not reflect the catalytically relevant state under PEC conditions. Consequently, reliable attribution requires correlative, operando methods that can track coordination/oxidation states and interfacial kinetics during illumination and bias, rather than relying on morphology alone. Operando synchrotron-based approaches (e.g. operando XAS) are increasingly used precisely for this purpose in photo(electro)catalysis [58].

The role of defect engineering and surface modification

Moving beyond the ideal structure, a powerful strategy for enhancing photoelectrocatalytic performance is the intentional introduction of imperfections through defect engineering and surface modification. Creating defects within the crystal lattice of the MOF-derived material, such as anion vacancies (e.g. oxygen vacancies in metal oxides), can profoundly alter its electronic and catalytic properties [59]. These vacancies can introduce new, localised electronic states within the semiconductor's bandgap, which can extend light absorption into the visible range. Furthermore, they can act as shallow traps for photogenerated charge carriers, promoting their separation and preventing immediate recombination [16]. Oxygen vacancies, in particular, are often implicated as active sites for water adsorption and activation, thereby lowering the kinetic barrier for the OER [60]. The central debate surrounding defect engineering is one of control; beneficial defects can also serve as recombination centres if their concentration and energy levels are not carefully managed [59].

In parallel with bulk defect engineering, surface modification via the deposition of cocatalysts remains a cornerstone strategy for improving PEC performance [61]. Cocatalysts are materials that, when deposited on the photoelectrode surface, provide more favourable active sites for the HER or OER, thereby reducing the activation energy (overpotential) required for these reactions [62]. While noble metals like platinum are highly effective HER cocatalysts, a major research thrust is the development of earth-abundant alternatives, such as MoS_2, NiP and CoP, many of which can be readily derived from MOF precursors [62]. A particularly sophisticated and emerging trend is the spatially selective deposition of cocatalysts on different components of a heterostructure. For example, in a ZnO/TiO_x composite (Fig. 6), an HER cocatalyst could be selectively placed on the TiO_x component (where electrons accumulate) and an OER cocatalyst on the ZnO component (where holes accumulate) [63]. This intelligent design directs the charge carriers to their designated reaction sites, minimising parasitic reactions and maximising overall efficiency.

Mechanistic distinctions between HER and OER across MOF-derived material classes

In MOF-derived PEC systems, the mechanistic requirements of the cathodic HER and anodic OER differ fundamentally, and these differences dictate which derived phases are a two-electron reaction proceeding through adsorbed hydrogen (H*) via

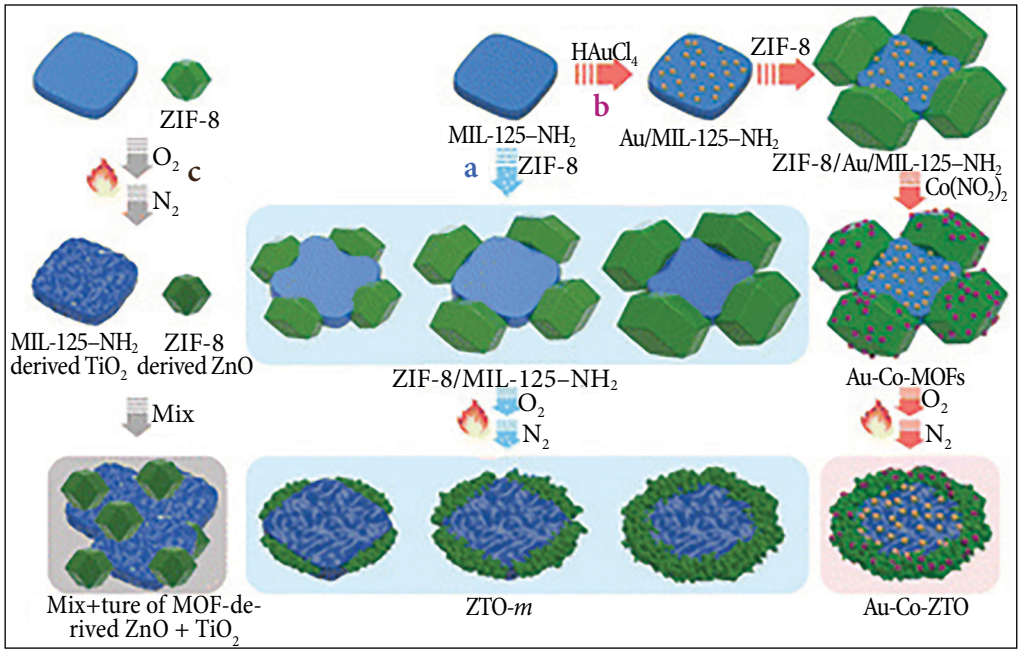

Fig. 6. Illustration showing the stepwise synthesis route to the fabrication of (a) ZTO-*m*, (b) Au-Co-ZTO, and (c) MOF-derived ZnO + TiO_2 mixture photocatalysts for CH_4 oxidation [63]

Volmer–Heyrovsky or Volmer–Tafel pathways, where the dominant kinetic bottleneck depends strongly on pH: in alkaline media, water dissociation (Volmer step) and OH* management become critical, whereas in acidic media proton reduction can be rate-determining depending on the catalyst surface [64]. By contrast, the OER is a four-electron, multi-step oxidation that proceeds through *OH, *O and *OOH intermediates; its activity is highly sensitive to the oxidation state and coordination environment of surface metal sites, and many transition-metal compounds (including MOF-derived phosphides/sulfides/selenides) operate as precatalysts that reconstruct under anodic bias to oxyhydroxide-like active phases (e.g. NiFeOOH/CoOOH), which are frequently the true OER-active species [65].

These mechanistic asymmetries translate into predictable material–function pairings in MOF-derived PEC design. MOF-derived oxides/hydroxides (or oxide-coated cocatalysts) are commonly favoured on photoanodes because they stabilise high-valent metal centres and promote OOH formation, whereas MOF-derived phosphides, sulfides, carbides, and N-doped carbon composites are often used on photocathodes/electrodes to provide a high conductivity and near-thermoneutral H adsorption, while also offering sites that facilitate water activation in alkaline HER. Importantly, when such phases are used as cocatalysts on a light absorber, their mechanistic role is typically to accelerate surface charge transfer and suppress surface recombination; only when the full two-electrode device is assembled this translates into an STH outcome [66].

PERFORMANCE, APPLICATIONS, AND OVERARCHING CHALLENGES

Bridging the gap between fundamental materials science and practical energy solutions requires a rigorous evaluation of performance and a clear-eyed assessment of the remaining obstacles. This section benchmarks the current state-of-the-art for MOF-derived photoelectrodes, examines their integration into complete hydrogen-producing devices, and critically discusses the significant challenges, particularly concerning stability and scalability, that must be overcome for this technology to achieve widespread impact.

Performance benchmarking of MOF-derived photoelectrodes

The efficacy of a photoelectrode is quantified by a set of key performance indicators measured under standardised conditions. The photocurrent density (Jph), typically measured at a potential of 1.23 V versus the reversible hydrogen electrode (RHE) for

photoanodes, represents the rate of charge carrier generation and collection under illumination (e.g. AM 1.5G, 100 mW/cm^2) [18]. The onset potential, the potential at which a discernible photocurrent appears, is a measure of the overpotential required to initiate the water splitting reaction; a more negative (cathodic) onset potential for photoanodes is desirable as it indicates lower energy losses [67]. Faradaic efficiency (ηF) confirms that the measured current corresponds to the desired chemical reaction (i.e. H_2 or O_2 production) rather than parasitic side reactions. Finally, long-term stability, assessed through chronoamperometry, measures the material's ability to maintain its performance over extended periods of operation [47].

Across the literature, MOF-derived materials have consistently demonstrated superior performance compared to both their pristine MOF precursors and many conventionally prepared semiconductor counterparts. For example, a $BiVO_4$ photoanode modified with a MOF-derived CoS cocatalyst achieved a remarkable photocurrent density of 5.22 mA/cm^2 at 1.23 V vs RHE, a significant enhancement over unmodified $BiVO_4$ [18]. Similarly, a photocathode based on MOF-derived FeP@C delivered a current density of 10 mA/cm^2 at a potential of –0.07 V vs RHE, showcasing an excellent HER activity [68]. These enhancements are a direct result of the design strategies discussed previously: the high surface area inherited from the MOF template maximises the electrode–electrolyte interface, the engineered heterojunctions promote charge separation, and the derived catalytic phases accelerate surface reaction kinetics. The tables below summarise the performance of several state-of-the-art MOF-derived photoanodes and photocathodes, providing a quantitative snapshot of the field's progress. Tables 2 and 3 provide a comparative summary of benchmark performance metrics for recently developed MOF-derived photoanodes and photocathodes, respectively. For photoanodes (Table 2), materials such as M-CoS/$BiVO_4$ and Co-BTC-BVO stand out, achieving high photocurrent densities of 5.22 and 4.82 mA/cm^2 at 1.23 V vs RHE. These examples underscore the success of MOF-derivation in creating highly active OER catalysts on established semiconductor scaffolds. Similarly, for photocathodes (Table 3), systems like S-CoWP@(S,N)-C demonstrate a remarkable HER activity, delivering a high current density of –35 mA/cm^2 at a minimal overpotential (–0.035 V). A critical observation across both tables is the wide variation in electrolyte conditions (ranging from acidic to alkaline and including sacrificial agents) and stability testing durations.

STH conversion and device integration

The ultimate metric for PEC water splitting technology is its solar-to-hydrogen (STH) conversion efficiency, which quantifies the percentage of incident solar energy that is successfully converted

Table 2. **Performance of state-of-the-art MOF-derived photoanodes (OER)**

Material system	Onset potential (V vs RHE)	Jph @ 1.23 V vs RHE, mA/cm^2	Electrolyte	Stability, h	Reference(s)
M-CoS/$BiVO_4$	~0.3	5.22	0.5 M $K_2H_2PO_4$ + Na_2SO_3	>2	[18]
Co-BTC-BVO	0.22	4.82	1 M KPi	>5	[69]
Fe_2O_3/MIL-88B@ZIF-67	~0.7	2.52	1 M NaOH	>10	[70]
TiO_2–Co_3O_4-450	~0.75	1.04	1 M NaOH	>1	[34]
T-Ni(OH)$_2$@TiO_2	~0.5	1.22	1 M KOH + urea	>2	[67]

Table 3. **Performance of state-of-the-art MOF-derived photocathodes (HER)**

Photocathode (MOF-derived)	Electrolyte	Photocurrent density (illumination)	Reference
NiO/carbon nanostructure (MOF-derived; QD-sensitised NiO–C)	Na_2SO_4 buffer (pH 6.8)	–0.0936 mA cm^{-2} at 0 V_RHE	[71]
Cu–Ni oxide nanomaterial derived from Cu-MOF-74	alkaline electrolyte (as reported)	~0.9 mA cm^{-2} (at 0.5 V_{RHE})	[72]
Hofmann-type MOF-derived CuNiOx photocathode	(as reported)	reported higher photocurrent vs CuO under illumination; stable during water photolysis	[73]

and stored as chemical energy in hydrogen fuel. The STH efficiency is typically calculated for a two-electrode system operating without any external electrical bias, using the formula

$$\eta STH = \frac{Jsc \times 1.23V \times \eta}{Pin},$$

where Jsc is the short-circuit photocurrent density, 1.23 V is the thermodynamic potential for water splitting, ηF is the Faradaic efficiency, and Pin is the power density of the incident light [74].

Achieving unbiased water splitting is extremely challenging for a single photoelectrode, as it is difficult for one material to both absorb enough light and generate sufficient photovoltage (>1.6–1.8 V in practice) to overcome all thermodynamic and kinetic barriers. Therefore, tandem concepts are being pursued along two closely related but distinct routes: PEC tandems, which couple a photoanode and a photocathode so that the two photoelectrodes jointly supply the photovoltage, and PV–electrolysis (PV–EC) tandems, where a high-efficiency photovoltaic device (e.g. perovskite, Si, or perovskite/Si) provides the photogenerated carriers and operating voltage, while the integrated catalysts – often MOF-derived – serve as electrocatalytic HER/OER electrodes [75]. In such a configuration, the photovoltages generated by the two photoelectrodes combine, enabling water splitting to be driven solely by solar energy. MOF-derived materials are beginning to play a crucial role in these advanced device architectures. In a landmark study, a tandem device was constructed by pairing a MOF-derived S-CoWP@(S,N)-C HER electrocatalyst with a lead halide perovskite solar cell, achieving an impressive STH efficiency of 10.98% [12]. Similarly, a monolithic perovskite/silicon tandem solar cell paired with a self-reconstructed NiCoFe-based hydroxide OER electrocatalyst achieved an STH efficiency of 21.32% in unbiased solar water splitting [76]. These results highlight the immense potential of integrating highly active MOF-derived (or MOF-enabled) electrocatalysts with high-performance photovoltaics to construct efficient, unbiased solar-fuel platforms.

Critical challenges and the path forward

While the performance metrics are promising, the path to practical application is contingent on addressing several fundamental and interconnected challenges. Table 4 provides a structured overview of these critical hurdles, mapping each problem – from a poor long-term stability and a low electrical conductivity to issues of scalability – to its underlying root cause and outlining promising mitigation strategies currently being explored by the research community. This framework serves as a roadmap for the subsequent discussion, which delves deeper into the nuances of these obstacles and the innovative solutions required to overcome them. Despite the remarkable progress, significant hurdles must be surmounted before MOF-derived photoelectrodes can be deployed in practical, large-scale technologies. The most critical of these is the 'stability bot-

Table 4. **Summary of key challenges and potential mitigation strategies**

Challenge	Root cause	Proposed strategy	Reference(s)
Poor long-term stability	Photocorrosion, chemical dissolution, mechanical stress from gas evolution	Deposition of protective layers (e.g. TiO_2, NiO_x); use of inherently stable precursors (e.g. Zr-MOFs); development of self-healing materials	[78]
Low electrical conductivity	Insulating nature of organic linkers in pristine MOFs; poor connectivity between derived nanoparticles	Pyrolysis to create conductive carbon matrix; hybridisation with graphene/MXene; synthesis of 1D nanostructures for direct transport pathways	[6]
Active site ambiguity	Complex composite nature (metal, carbon, interface); *in situ* structural changes during operation	Advanced operando characterisation (XAS, Raman); high-level DFT calculations to model reaction pathways on different sites	[53]
Scalability and cost-effectiveness	Complex, multi-step, lab-scale synthesis; use of expensive reagents or solvents	Development of continuous flow, microwave-assisted, or mechanochemical synthesis methods; focus on earth-abundant precursors	[79]
Lack of standardised reporting	Variation in light sources, electrolytes, cell setups, and stability test durations across labs	Community adoption of standardised protocols for PEC measurements and reporting to enable reliable comparison of materials	[78]

tleneck'. While the literature is replete with reports of a high initial activity, the long-term durability of these materials is often the limiting factor [6]. The operating conditions of PEC water splitting are exceptionally harsh: the photoelectrode is subjected to a corrosive aqueous electrolyte (either strongly acidic or alkaline), intense solar irradiation that can induce photocorrosion, and the physical stress of continuous gas bubble evolution from its surface. This often leads to a fundamental activity-stability trade-off, where the most catalytically active surface species or defect sites are also the most chemically unstable and prone to degradation or reconstruction into less active phases [77]. Achieving the multi-year lifetimes required for economic viability (e.g. a five-year target) is a far greater challenge than achieving a high initial efficiency, and will require a research pivot towards developing more robust materials, such as those derived from highly stable Zr-based MOFs, and designing effective protective layers that can shield the active material from the electrolyte without impeding charge transfer [15].

Beyond stability, the issues of scalability and cost present major barriers to commercialisation. Many of the sophisticated, multi-step synthesis procedures used to create high-performance hierarchical nanostructures are confined to the laboratory scale and rely on expensive or specialised reagents and equipment [80]. Developing cost-effective, scalable and reproducible synthesis methods, such as continuous flow reactors or microwave-assisted synthesis, will be essential for producing these materials in the quantities needed for industrial application [81]. Finally, the field suffers from a lack of standardised testing and reporting protocols. Variations in illumination sources, electrolyte conditions, reactor configurations, and stability testing durations make it exceedingly difficult to perform direct, meaningful comparisons of performance between different studies. The adoption of a community-wide set of standards for evaluating and reporting data is crucial for accelerating progress and identifying the most genuinely promising material systems [78].

CONCLUSIONS

The strategic use of metal-organic frameworks as sacrificial templates has unequivocally established itself as a powerful and versatile paradigm for the design of advanced photoelectrode materials for PEC water splitting. This review has charted the progress of the field, demonstrating how the controlled thermal transformation of MOFs enables the synthesis of materials that successfully overcome the critical limitations of poor conductivity and stability inherent to pristine MOFs. By inheriting the high surface area and tunable morphology of their precursors, MOF-derived materials – ranging from porous metal oxides to single-atom catalysts embedded in nitrogen-doped carbon – exhibit significantly enhanced performance. The rational design of these materials, through the careful selection of MOF precursors, precise control over derivatisation conditions, and the intelligent construction of heterostructures, has been shown to be paramount for optimising light absorption, promoting charge separation, and accelerating surface reaction kinetics.

Despite these significant achievements, the journey towards practical, large-scale solar hydrogen production is still fraught with challenges. The central issue remains the activity-stability trade-off, where achieving long-term operational durability in harsh electrochemical environments is the ultimate frontier. Looking ahead, the continued advancement of this field will likely be driven by several emerging trends and research directions. The pursuit of ultimate atomic efficiency will propel further research into MOF-derived single-atom catalysts (SACs). The ability to stabilise individual metal atoms in a conductive matrix offers the potential for unprecedented catalytic activity and selectivity, and overcoming the current challenges in their synthesis and long-term stability could lead to breakthrough performance. To guide these synthetic efforts, a deeper integration of advanced characterisation and computational modeling is essential. The use of *in situ* and *operando* techniques, such as ambient pressure XPS and time-resolved X-ray absorption spectroscopy, coupled with high-throughput DFT calculations, will be critical for unravelling complex, dynamic reaction mechanisms at the catalyst surface and identifying the true nature of the active sites under operational conditions.

Furthermore, the design principles and material systems developed for water splitting are readily transferable to other crucial solar fuel reactions. The photoelectrochemical reduction of CO_2 into valuable fuels and chemical feedstocks (e.g. methane, methanol and ethylene) represents a parallel

grand challenge, and MOF-derived materials are already showing an immense promise in this area. Finally, as the combinatorial complexity of potential MOF precursors and synthesis conditions becomes increasingly vast, traditional Edisonian approaches to materials discovery will become inefficient. The integration of artificial intelligence and machine learning algorithms to screen virtual libraries of MOFs, predict their derived properties, and optimise synthesis parameters offers a transformative path to accelerate the discovery of next-generation photoelectrode materials. By embracing these future directions, the field of MOF-derived materials is poised to make substantial contributions to the development of a sustainable energy future powered by solar fuels.

Received 5 January 2026
Accepted 8 February 2026

References

1. E. S. Sowbakkiyavathi, P. Dhandapani, S. Ramasamy, et al., *RSC Sustainability*, **3**, 3628 (2025).
2. P. P. Danita, R. V. Solomon, *Energy Adv.*, **4**, 597 (2025).
3. C. Tang, X. Li, Y. Hu, et al., *Molecules*, **29** (2024).
4. N. Zaman, N. Iqbal, T. Noor, *Arab. J. Chem.*, **15** (2022).
5. G. Valdebenito, M. González-Carvajal, L. Santibañez, et al., *Catalysts*, **12** (2022).
6. S. H. A. Shah, A. Shah, F. J. Iftikhar, *ACS Appl. Nano Mater.*, **7**, 8424 (2024).
7. Z. Wang, H. Yang, D. Zhang, et al., *Nanoscale* (2025).
8. L. Oar-Arteta, T. Wezendonk, X. Sun, et al., *Mater. Chem. Front.*, **1**, 1709 (2017).
9. G. Shen, M. Li, Y. Chen, et al., *Catalysts*, **13** (2023).
10. B. An, K. Cheng, C. Wang, et al., *ACS Catal.*, **6**, 3610 (2016).
11. J. A. Powell, H. Lin, Y. Yang, et al., *Cryst. Growth Des.*, **25**, 1256 (2025).
12. B. Weng, C. R. Grice, W. Meng, et al., *ACS Energy Lett.*, **3**, 1434 (2018).
13. M. Z. Hussain, Z. Yang, B. van der Linden, et al., *Energy Fuels*, **36**, 12212 (2022).
14. K. Chen, C.-D. Wu, *Angew. Chem. Int. Ed.*, **58**, 8119 (2019).
15. X. Li, Z. Shao, Y. Zhang, et al., *Nano Res.*, **18**, 94907403 (2025).
16. Y. Zhang, F. Mao, L. Wang, et al., *Solar RRL*, **4**, 1900438 (2020).
17. S. Feng, S. Fan, L. Li, et al., *Nano Res. Energy*, **3**, e9120117 (2024).
18. D. Li, X. Chen, M. Shao, et al., *J. Mater. Chem. A*, **13**, 22652 (2025).
19. M. Yuan, R. Wang, Z. Sun, et al., *Inorg. Chem.*, **58**, 11449 (2019).
20. G. Jia, L. Liu, L. Zhang, et al., *Appl. Surf. Sci.*, **448**, 254 (2018).
21. Y.-H. Nien, X.-H. Chen, J.-C. Chou, et al., *IEEE Sens. J.*, **25**, 30351 (2025).
22. W. He, X. Guo, J. Zheng, et al., *Inorg. Chem.*, **58**, 7255 (2019).
23. X. San, G. Zhao, G. Wang, et al., *RSC Adv.*, **7**, 3540 (2017).
24. Z. Xiao, Y. Mei, S. Yuan, et al., *ACS Nano*, **13**, 7024 (2019).
25. J. Yao, J. Qian, D. Yu, et al., *Appl. Surf. Sci.*, **654**, 159457 (2024).
26. C. Liu, X. Shen, G. Johnson, et al., *Front. Chem.*, **8** (2020).
27. L. Wang, Z. Liu, J. Zhang, et al., *Chin. Chem. Lett.*, **34**, 108007 (2023).
28. N. Q. Tran, T. T. Truong, T. T. N. Tran, et al., *ACS Sustainable Chem. Eng.*, **12**, 1038 (2024).
29. C. Li, T. Hang, H. Zhou, et al., *Inorg. Chem. Front.*, **10**, 3375 (2023).
30. Q. Ding, L. Gou, D. Wei, et al., *Int. J. Hydrogen Energy*, **46**, 24965 (2021).
31. S. Zhong, B. Kang, X. Cheng, et al., *ACS Sustainable Chem. Eng.*, **12**, 1233 (2024).
32. B. Tahir, A. Alraeesi, M. Tahir, *Front. Chem.*, **12** (2024).
33. P. A. Koyale, A. D. Patil, T. D. Dongale, et al., *J. Mater. Chem. C*, **12**, 12499 (2024).
34. C. T. T. Thanh, H. J. Jo, G. Koyyada, et al., *Materials*, **16**, 5461 (2023).
35. S. Zhong, B. Kang, X. Chen, et al., *ACS Sustainable Chem. Eng.*, **12**, 1233 (2024).
36. M. Liu, L.-Z. Qiao, B.-B. Dong, et al., *Appl. Catal. B Environ.*, **273**, 119066 (2020).
37. Q. Liu, C. Wang, H. Wang, et al., *Int. J. Hydrogen Energy*, **81**, 66 (2024).
38. Y. Sun, Y. Wang, D. Liu, et al., *ACS Appl. Mater. Interfaces*, **17**, 14278 (2025).
39. H. Yin, T. Zhan, J. Chen, et al., *J. Mater. Sci. Mater. Electron.*, **31**, 4323 (2020).
40. T. Hou, Z. Jia, B. Wang, et al., *Chem. Eng. J.*, **422**, 130079 (2021).
41. G. Qin, J. Zheng, Y. Li, et al., *J. Colloid Interface Sci.*, **615**, 432 (2022).
42. H.-L. Jiang, B. Liu, Y.-Q. Lan, et al., *J. Am. Chem. Soc.*, **133**, 11854 (2011).
43. D. Givirovskaia, G. Givirovskiy, V. Laitinen, et al., *Nano Res.*, **18**, 94907100 (2025).
44. X.-J. Tian, S.-J. Guo, Z.-Y. Wu, et al., *Mater. Horiz.* (2025).
45. B. Gibbons, D. R. Cairnie, B. Thomas, et al., *Chem. Sci.*, **14**, 4672 (2023).
46. W. Rehman, F. Saeed, S. Arain, et al., *J. Compos. Sci.*, **9**, 250 (2025).
47. S.-M. You, W. M. A. El Rouby, L. Assaud, et al., *Hydrogen*, **2**, 58 (2021).

48. B. Gibbons, D. R. Cairnie, B. Thomas, et al., *Chem. Sci.*, **14**, 4672 (2023).
49. G. Dong, T. Chen, F. Kou, et al., *Nanomaterials*, **14**, 1100 (2024).
50. J. Pan, B. Wang, J. Wang, et al., *Angew. Chem. Int. Ed.*, **60**, 1433 (2021).
51. D. Li, X. Chen, M. Shao, et al., *J. Mater. Chem. A*, **13**, 22652 (2025).
52. C. Feng, L. Liu, H. Fu, et al., *Catal. Sci. Technol.*, **14**, 4860 (2024).
53. J. Canivet, M. Vandichel, D. Farrusseng, *Dalton Trans.*, **45**, 4090 (2016).
54. Z. Zhai, W. Yan, L. Dong, et al., *J. Mater. Chem. A*, **9**, 20320 (2021).
55. D. Guo, R. Shibuya, C. Akiba, et al., *Science*, **351**, 361 (2016).
56. Y. Pan, S. Liu, K. Sun, et al., *Angew. Chem. Int. Ed.*, **57**, 8614 (2018).
57. Y. Miao, J. Liu, L. Chen, et al., *Chem. Eng. J.*, **427**, 131011 (2022).
58. M. A. Soldatov, P. V. Medvedev, V. Roldugin, et al., *Nanomaterials*, **12**, 839 (2022).
59. Z. Fang, B. Bueken, D. E. De Vos, et al., *Angew. Chem. Int. Ed.*, **54**, 7234 (2015).
60. F. Chen, X. Mu, J. Zhou, et al., *Chin. J. Chem.*, **42**, 2520 (2024).
61. W. Ma, L. Yu, P. Kang, et al., *Molecules*, **29** (2024).
62. W. Wang, X. Xu, W. Zhou, et al., *Adv. Sci.*, **4**, 1600371 (2017).
63. W. Zhao, K. Sun, J. Xu, et al., *Chem. Sci.* (2025).
64. A. Lasia, *Int. J. Hydrogen Energy*, **44**, 19484 (2019).
65. J. Y. C. Chen, L. Dang, H. Liang, et al., *J. Am. Chem. Soc.*, **137**, 15090 (2015).
66. L. Su, S. Zhang, H. Wu, et al., *Nano Energy*, **130**, 110177 (2024).
67. J. Ren, P. Yang, L. Wang, et al., *Catalysts*, **13** (2023).
68. S. C. Shit, I. Mondal, S. Pendem, et al., *ChemElectroChem*, **5**, 2842 (2018).
69. Y. Li, X. Dai, Y. Bu, et al., *Small*, **18**, 2200454 (2022).
70. X. Shi, J. Zhu, T. Bai, et al., *Chem. J. Chin. Univ.*, **43**, 20210613 (2022).
71. L. Shi, D. Benetti, F. Li, et al., *Small*, **18**, 2201815 (2022).
72. M. Bouchabou, J. M. R. López, M. D. C. Román Martínez, et al., *ACS Appl. Nano Mater.*, **8**, 8646 (2025).
73. L. Trinh, K. Bienkowski, A. Parzuch, et al., *Int. J. Hydrogen Energy*, **87**, 1171 (2024).
74. H. Döscher, J. L. Young, J. F. Geisz, et al., *Energy Environ. Sci.*, **9**, 74 (2016).
75. B. Liu, S. Wang, G. Zhang, et al., *Chem. Soc. Rev.*, **52**, 4644 (2023).
76. S. Pan, R. Li, Q. Zhang, et al., *J. Mater. Chem. A*, **9**, 14085 (2021).
77. H. Tang, D. Fan, Y. Chen, et al., *Green Chem.*, **27**, 2605 (2025).
78. M. Xiao, Z. Wang, K. Maeda, et al., *Chem. Sci.*, **14**, 3415 (2023).
79. M. Ali, E. Pervaiz, O. Rabi, *ACS Omega*, **6**, 34219 (2021).
80. S. Feng, S. Wen, R. Wang, et al., *Nanomaterials*, **15**, 841 (2025).
81. K. Ahmad, T. H. Oh, *Chemosensors*, **13** (2025).

Min Mei, Wenjing Yang

MOF KILMĖS MEDŽIAGOS FOTOELEKTROCHEMINIAM VANDENS SKAIDYMUI: PROJEKTAVIMO PRINCIPAI, MECHANIZMAI IR SAULĖS ENERGIJOS PANAUDOJIMAS VANDENILIO GAMYBAI